PHYSICAL REVIEW C VOLUME 27, NUMBER 2 FEBRUARY 1983

Angular distributions of relativistic alpha particles in heavy-ion collisions

M. M. Aggarwal, K. B. Bhalla, G. Das, and P. L. Jain
High Energy Experimental Laboratory, Department of Physics, State University of New York at Buffalo, Buffalo, New York 14260
(Received 26 April 1982)

Angular distributions of relativistic α particles produced from Fe emulsion and Ar emulsion at about $2A$ GeV and Fe emulsion at $0.9A$ GeV have been studied. The angular distribution falls in either one or the other of two separate classes with different characteristics; hot for tail or cold for peak zones, and thus, a single Boltzmann distribution cannot fit the fragmentation peak and the tail simultaneously. Two zones are characterized by separate Boltzmann distributions in the projectile rest frame and the associated temperatures differ by a factor of 4 or more. The α particles with large angular distributions especially cannot be explained by a model which is based on the fragmentation from a clean-cut participants-spectator picture. Experimental results in the "hot" events give some direct evidence for the transfer of large "transverse" momenta in these collisions.

[NUCLEAR REACTIONS Ar or (Fe) + em$\rightarrow\alpha+x$, $E=1A$ GeV and $2A$ GeV. Angular distribution of α particle, Fermi momentum and Maxwell-Boltzmann parametrization.]

I. INTRODUCTION

Recently much experimental and phenomenological effort has been devoted towards the investigation of relativistic heavy-ion collisions. On account of the complex nature of these collisions, only the multiplicity and the single-particle inclusive spectra have been commonly studied. But it is well known that nuclear emulsion detectors have by far the highest spatial resolution of any particle detectors. It is a 4π detector and allows an exclusive type of analysis on an event by event basis. In the current experiment we shall study the angular distributions of relativistic α particles produced in the interactions of Fe emulsion at $2A$ and $0.9A$ GeV and Ar emulsion at $2A$ GeV. The α particles are easily identified by their distinct grain density and/or by their δ-ray density measurements. In Sec. III A, pure projectile fragmentation events are analyzed. Different parameters such as momentum width, Fermi momentum, and temperature for excitation are calculated for Ar and Fe projectiles and these results are compared with similar results for CNO reactions. Section III B deals with angular distributions for a general sample (all N_h) and these distributions are compared for different N_h groups. Experimental distributions are compared with the theoretical predictions of moving relativistic Boltzmann distributions. Assuming α particles are emitted from a fireball (thermal source), the velocity (β) and the temperature (T) of the involved sources are calculated for different cases. We also discuss the dependence of angular distributions on the fragmentation of the projectile (number of α particles, etc.). An attempt is also made in Sec. III D to isolate the events responsible for the tail part of the angular distribution produced by Fe as well as by Ar beams. We find that in general there is a trend that the events fall in either one or the other of two different classes with different characteristics in the "hot" or "cold" zones. Each of these classes is characterized by a Boltzmann distribution in the projectile rest frame but is associated with two distinct temperatures differing by a factor of 4 or 5. Our experimental results on hot events could be explained through a transverse momentum transfer to the spectator before fragmentation.

II. EXPERIMENTAL TECHNIQUES

In this experiment, we used two stacks of Ilford G-5 emulsion pellicles 600 cm thick and of the dimensions 12×8 cm^2 and 10×10 cm^2 exposed to ^{56}Fe and ^{40}Ar beams at $2A$ GeV. We also used a third emulsion stack of the dimension 10×10 cm^2 exposed to a ^{56}Fe beam at a low energy of $0.9A$ GeV. Each stack was exposed parallel to the pelli-

cle surfaces. Each pellicle was scanned by the along-the-track method,[1,2] under high magnification. In this experiment we used 975 interactions from Fe and Ar beams at high energies and 900 interactions from an Fe beam at low energy. From these events we separated the "pure" projectile fragmentation events known as "white stars" with $N_h=0$, where N_h is the number of nonrelativistic particles emitted from the interactions with $\beta \leq 0.7$. From these interactions we identified and measured the relativistic α particles making angles up to 15° with respect to the beam direction (θ_L). The velocity of α particles emitted in the forward cone should be very close to the velocity of the projectile. Thus the α particle should have a grain density where $g_\alpha \sim 4g_{\min}$ and for relativistic tracks it should not change within 2 cm of its path length followed from its production point. On the other hand, if the track with a grain density that is approximately $4g_{\min}$ is due to singly charged slow particles (p, d, or t), the track will either stop or its ionization will change appreciably after traveling 2–3 cm. All the α particle tracks were followed for another part of an experiment,[2] and it was observed that the contamination of singly charged particles in $4g_{\min}$ tracks is negligibly small ($<0.5\%$). All the α particles making an angle of 10° for higher energies (Fe and Ar beams) and 15° for lower energy (Fe beam) interactions, with the beam tracks were thus identified. The multiplicity of relativistic α particles, N_α, produced in each interaction was also recorded.

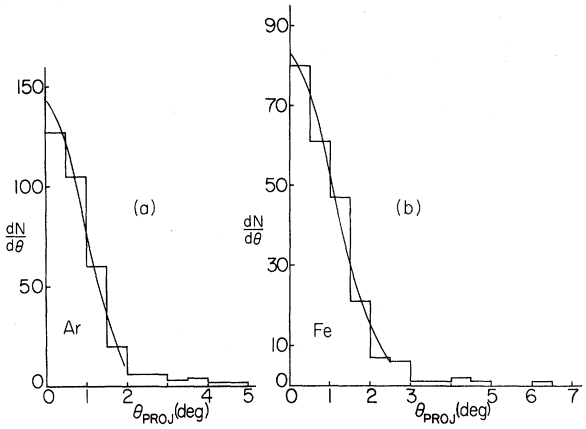

FIG. 1. Projected angle distributions for relativistic α particles for pure projectile fragmentation, $N_h=0$ events; (a) ^{40}Ar reaction at $2A$ GeV and (b) ^{56}Fe reaction at $2A$ GeV. Curves correspond to a fit due to the equation $N(\theta)=Ae^{-\theta^2/2\sigma^2}$.

III. RESULTS AND DISCUSSION

A. Projected angular distribution of helium projectile fragments

In Sec. I we mentioned white stars as events with no visible target fragmentation ($N_h=0$) and these events are generally considered to be produced at large impact parameters. In Fig. 1 the observed projected angular distributions for relativistic α particles produced in $N_h=0$ type reactions of Ar and Fe in nuclear emulsions at higher energies ($\sim 2A$ GeV) are shown. One notices that both these angular distributions are dominated by narrow forward peaks having a characteristic width of ~ 1 deg. There are some α particles scattered at larger angles than expected from the pure projectile fragmentation process. Projected angular distributions are fitted with a single Gaussian distribution $\sim e^{-\theta^2/2\sigma^2(\theta)}$. The angular distribution for ^{56}Fe reactions is slightly broader than that for ^{40}Ar reactions, with the widths being $\sigma(\theta)_{\text{Fe}}=1.09\pm0.06$ and $\sigma(\theta)_{\text{Ar}}=0.89\pm0.03$, respectively. Both these widths are higher than $\sigma(\theta)=0.64\pm0.2$ that were observed for α particles from[3] ^{12}C, ^{14}N, and ^{16}O. Thus, we find that the projected angular distributions of α secondaries are well described by the single Gaussian, and the standard deviations of $\sigma(\theta_{\text{proj}})$ are in reasonable agreement with the theory of Lepore and Riddell.[4]

The experimentally observed values of $\sigma(\theta)$ can be related to $\sigma(p)$, the width of momentum distribution, in the projectile frame by the relation

$$\sin[\sigma(\theta)]=[\sigma(p)A_B/(p_B A_F)] , \tag{1}$$

where p_B is the beam momentum per nucleon, and A_B and A_F are the mass numbers of the beam and fragment nuclei, respectively. $\sigma(p)$ can be calculated by using the formulation of Lepore and Riddell.[4] They treated the fragmentation of high energy nuclei by using a quantum mechanical sudden approximation and thus deduced the following expression for $\sigma(p)$:

$$\sigma(p)=[m_n(45A_B^{-1/3}-25A_B^{-2/3})A_F(A_B-A_F)/2A_B]^{1/2}\ \text{MeV} , \tag{2}$$

TABLE I. Comparison of experimental and theoretical parameters used in the projected angular distribution at $\sim 2A$ GeV.

Beam	Reference	Observed $\sigma(\theta)$ in deg	Observed $\sigma(p)$ in MeV/c	Calculated (Ref. 4) Eq. (2) $\sigma(p)$	Calculated (Ref. 4) Eq. (2) $\sigma(\theta)$	Fermi momentum (Ref. 6) Eq. (3) MeV/c	Temperature T (Ref. 6) Eq. (4) MeV
Ar	This work	0.89±0.03	179.5	^{3}He 120	0.89		
				^{4}He 136.5	0.76	209	9.5
					Combined 0.79	(251)[a]	
Fe	This work	1.09±0.06	220	^{3}He 116	0.86		
				^{4}He 132	0.74	252	13.8
					Combined 0.77	(260)[a]	
C, N, O	Ref. 3	0.64±0.02	129	^{3}He 126	0.84	185±3 (Ref. 3)	7.8±0.3 (Ref. 3)
				^{4}He 138	0.69	for ^{16}O reaction	

[a]Fermi momentum obtained from electron scattering experiment (Ref. 7).

where A_B is the mass number of the beam and m_n is the nucleon mass. The observed momentum widths can be related to the Fermi momentum p_f if sudden emission of virtual α clusters is assumed according to the picture of Feshback and Huang.[5] Using the formulation of Goldhaber,[6] the relation between $\sigma(p)$ and p_f comes out of the form

$$\sigma^2(p)=(p_f{}^2/5)[A_F(A_B-A_F)/(A_B-1)] . \quad (3)$$

Assuming that after excitation the nucleus comes to thermal equilibrium at temperature T, the observed value of $\sigma(p)$ can be related to temperature T by the following relation:

$$KT=(\sigma^2(p)A_B)/[m_nA_F(A_B-A_F)] . \quad (4)$$

Experimental and calculated values of $\sigma(\theta)$ and $\sigma(p)$ and the derived values of p_f and T [Eqs. (3) and (4)] are given in Table I, along with respective values for C, N, and O projectiles for comparison.[3] We notice that the values of the Fermi momentum obtained in this experiment for different projectiles are quite comparable with the values obtained by electron scattering experiments.[7] The values of p_f used in Table I were obtained by interpolating the results of Moniz *et al.*[7] The values of the excitation energy KT are also comparable to the binding energy per nucleon of the projectile, indicating that very little energy transfer takes place between the target and the fragment during a fragmentation process.

In Fig. 2 we display the projected angular distribution of α particles as a function of target nucleus $N_h \leq 6$ for H, C, N, and O and $N_h > 6$ for Ag and Br for a ^{40}Ar beam at $2A$ GeV. By comparing these two distributions with Fig. 1(a) for $N_h=0$, we find no difference in the widths of these distributions in

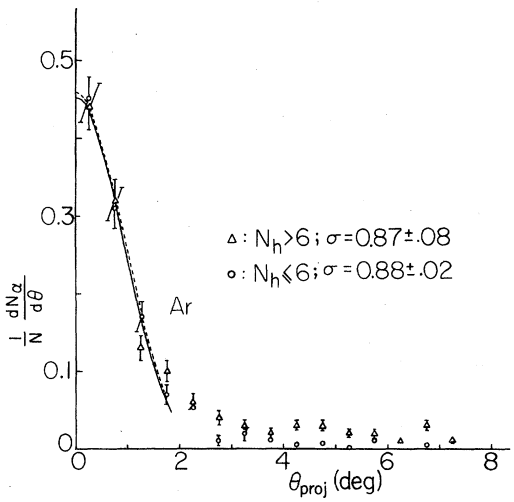

FIG. 2. Projected angle distributions for relativistic α particles as a function of target nucleus $N_h \leq 6$ (0) for H, C, N, and O, and $N_h > 6(\Delta)$ for Ag and Br for ^{40}Ar beams at $2A$ GeV. The curves correspond to a fit due to the equation $N(\theta)=Ae^{-\theta^2/2\sigma^2}$.

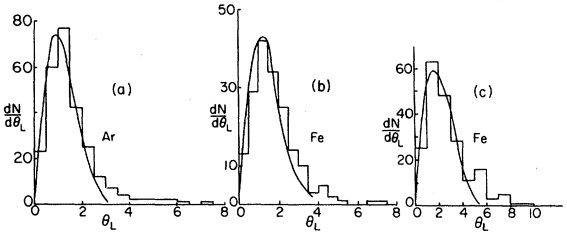

FIG. 3. Histograms are space angle distributions for $N_h=0$ events for (a) Ar reactions at $2A$ GeV, (b) Fe reactions at $2A$ GeV, and (c) Fe reactions at $0.9A$ GeV. The curves are from the moving Boltzmann distribution [Eq. (6)].

the projectile fragmentation region. Their projected angular widths are 0.89, 0.88, and 0.87, respectively. This target-independent behavior of the angular widths is a characteristic feature of the hypothesis of limiting fragmentation.

B. Space angle distribution of helium projectile fragments

In Figs. 3(a)–3(c) the angular distributions for "white" stars ($N_h=0$) for ^{40}Ar ($\sim 2A$ GeV), ^{56}Fe ($\sim 2A$ GeV), and ^{56}Fe ($0.9A$ GeV) beams, respectively, are shown. Very few α particles have angles greater than $\sim 3°$ and thus we can define the number of alpha particles in a tail to peak ratio R_{tp} as

$$R_{tp}=\frac{\theta_p<\theta_\alpha\leq\theta_t}{\theta\alpha\leq\theta_p}\ . \tag{5}$$

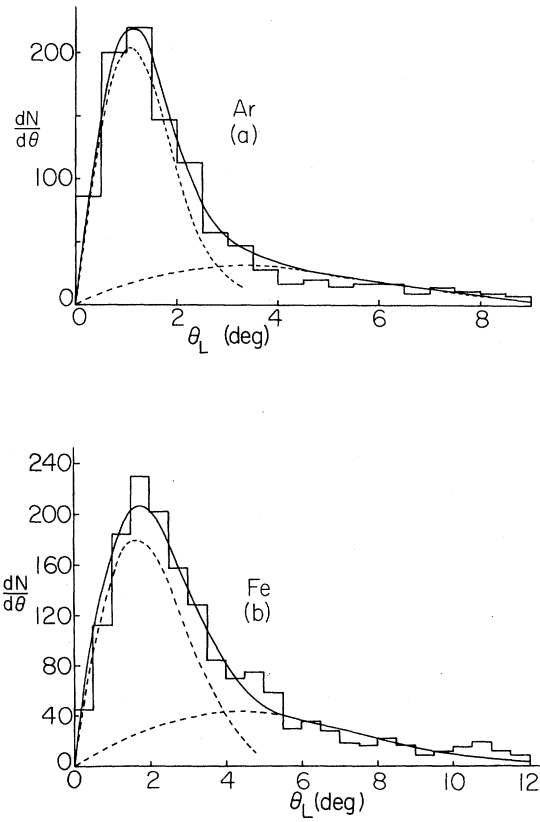

FIG. 4. Histograms are space angle distributions for $N_h>0$ events for (a) Ar reactions at $2A$ GeV and (b) Fe reactions at $0.9A$ GeV. The curves are from the moving Boltzmann distributions [Eq. (6)], dotted line curves are for peak or tail regions, and full line curves are for the sum.

TABLE II. Values of different parameters observed in different kinds of interactions.

Beam	Energy (GeV)	Sample	R_{tp}	T_t	β_t	T_p (MeV)	Reference
Fe	$0.9A$	$N_h=0$	0.22±0.04			9	
		$N_h\geq 0$	0.39±0.02	40	0.81	8	This work
		$1\leq N_h\leq 6$	0.27±0.02	33	0.81	8	
		$N_h>6$	0.59±0.04	48	0.80	9	
Fe	$1.7A$	$N_h=0$	0.10±0.02			7	
		$N_h\geq 0$	0.38±0.02	52	0.92	12	Ref. 8
		$1\leq N_h\leq 6$	0.29±0.04	34	0.92	12	
		$N_h>6$	0.54±0.05	60	0.91	10	
Ar	$2A$	$N_h=0$	0.14±0.03			7	
		$N_h\geq 0$	0.27±0.18	68	0.92	9	This work
		$1\leq N_h\leq 6$	0.24±0.03	57	0.92	10	
		$N_h>6$	0.41±0.04	78	0.91	7	

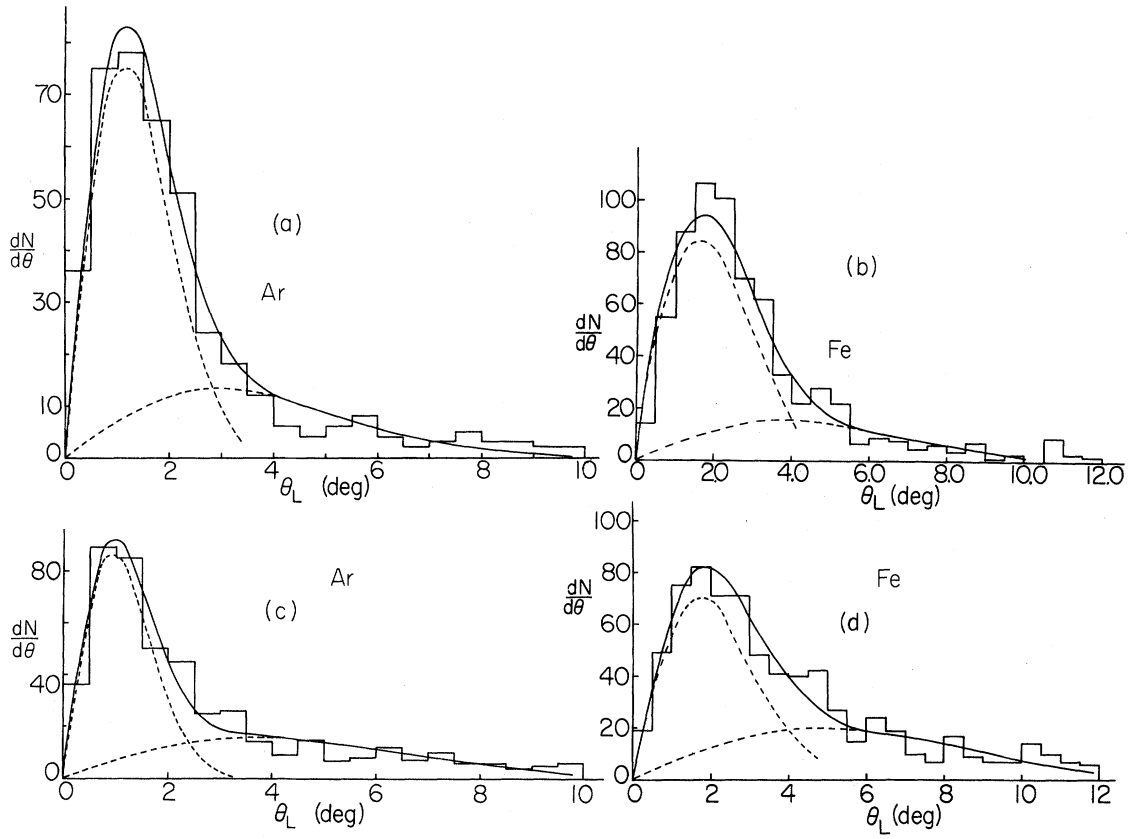

FIG. 5. Histograms are space angle distributions: (a) and (b) are for $1 \leq N_h \leq 6$ for Ar and Fe reactions, respectively. (c) and (d) are for $N_h > 6$ for Ar and Fe reactions, respectively. The curves are calculated from Eq. (6), dotted line curves represent peak or tail regions, and full line curves are for the sum.

For comparison purposes, we show in Figs. 4(a) and (b) the angular distributions for a general sample of reactions (all N_h). We have taken $\theta_p = 3°$ and $\theta_t = 10°$ for Ar at $2A$ GeV, and $\theta_p = 4°$ and $\theta_t = 12°$ for Fe at $0.9A$ GeV. The value of R_{tp} for all cases is summarized in Table II. Distributions in Fig. 4 exhibit broader peaks and much larger tails than those corresponding distributions observed in Fig. 3 with $N_h = 0$. Reactions with all N_h events indicate a substantial number of α particles with emission angles much greater than those expected from fragmentation of a clean cut spectator. The values of R_{tp} for ^{56}Fe beams at two different energies are remarkably the same and are higher than those for the lower beam mass of Ar.

In Figs. 5(a)–5(d) the angular distributions for two N_h groups, i.e., $1 \leq N_h \leq 6$ and $N_h > 6$, for Ar and Fe beams, respectively, are shown. For the Ar beam one observes a slightly broader fragmentation peak for the $1 \leq N_h \leq 6$ group and that the tail seems to be larger for the $N_h > 6$ group (see Table II). On the other hand, for the Fe beam at a lower energy ($0.9A$ GeV), events with $N_h > 6$ exhibit a slightly broader fragmentation peak as well as a larger tail as compared to events with $1 \leq N_h \leq 6$.

C. Fireball formalism

In order to understand the mechanism of the production of large angle α particles, the experimental distribution is fitted to the prediction of moving the relativistic Boltzmann distribution. Here the α particles are assumed to be emitted from a fireball (thermal source) which is formed by the nucleons mutually swept out from the target and the projectile during a collision between heavy ions. This fireball is moving with a velocity β and has reached a state of thermal equilibrium at temperature T (MeV). No assumption is made regarding the for-

mation mechanism of the fireball or the thermal source from which α particles are assumed to be emitted. Assuming the Boltzmann distribution as the probability distribution in the rest frame of the fireball, Gosset *et al.*,[9] obtained the following expression for the angular distribution in the laboratory frame, i.e., the moving relativistic Boltzmann distribution:

$$\frac{dP}{d\theta_L}=\frac{\gamma\sin\theta_L}{2I(\alpha)}\left\{\frac{4\eta e^{-\chi}}{(1-\eta^2)^2}\left[\frac{1}{\chi^2}+\frac{1}{\chi^3}\right]+\frac{\eta e^{-\chi}}{(1-\eta^2)}\left[\frac{1}{\chi}+\eta^2\right]\right.$$
$$\left.+\frac{(1+\eta^2)}{(1-\eta^2)\chi}\left[k_0(x,t_L)+\frac{2}{x}k_1(x,t_L)\right]+\frac{\eta^2}{(1-\eta^2)^{1/2}}k_1(x,t_L)\right\}. \quad (6)$$

Various variables used in Eq. (6) are defined as

$$\alpha=\frac{m}{T},\ \chi=\gamma\alpha,\ \eta=\beta\cos\theta_L,\ x=\chi\sqrt{1-\eta^2},\ t=\ln[(1-\eta)/(1+\eta)]^{1/2},$$
$$k_0(x,t_L)=\int_{t_L}^{\infty}e^{-x\cosh u}du,\ k_1(x,t_L)=\int_{t_L}^{\infty}e^{x\cosh u}\sinh^2 u\,du,$$
$$I(\alpha)=\frac{2}{\alpha^2}k_1(\alpha,0)+\tfrac{1}{2}k_0(\alpha,0),$$

where m is the mass of the α particle and θ_L is the space angle in the laboratory frame.

The calculated angular distributions, shown as curves in Figs. 3–5, are obtained using relation (6). For $N_h=0$ events, which are representative samples of pure projectile fragmentation events, experimental angular distributions should fit to those calculated for $\beta=\beta_p$, the projectile velocities, and temperatures about 7–8 MeV. The curves shown in Figs. 3(a)–3(c) correspond to temperature 7 MeV (Ar), 7 MeV (Fe 2A GeV), and 9 MeV (Fe 0.9A GeV), respectively, and are obtained by minimizing the χ^2 between the experimental and calculated numbers using T as a free parameter. We can see that experimental distributions are well explained, if α particles are assumed to be emitted by the pure projectile fragmentation process; of course there are some α particles scattered at large angles or in the tail area.

Other angular distributions (Figs. 4 and 5) are fitted to theoretical curves which are obtained by the superposition of two Boltzmann distributions, one for the tail area and the other for the peak area. The experimental distribution in the tail region θ_p to θ_t is first fitted to relativistic Boltzmann distributions with β and T as free parameters. Many sets of T and β values give a good fit (i.e., χ^2 is nearly minimum). β, T values which fit experimental distributions of Figs. 4 and 5 are plotted as "expt. fit" curves in Fig. 6 for different N_h values. All these values of β and T are not permissible. Yet it is assumed that N_p (the number of nucleons from the projectile) and N_t (the number of nucleons from the target), somehow come together and share the available energy to form a completely thermalized fireball. Using this picture, kinematically allowed values of β and T can be calculated by four-momentum conservation in the following manner:

$$\beta=\frac{P_L}{E_L}=\frac{N_p[k(k+2m')]^{1/2}}{(N_p+N_t)m'+N_pk}, \quad (7)$$

where k is the kinetic energy (KE) of the projectile per nucleon and m' is the mass of the bound nu-

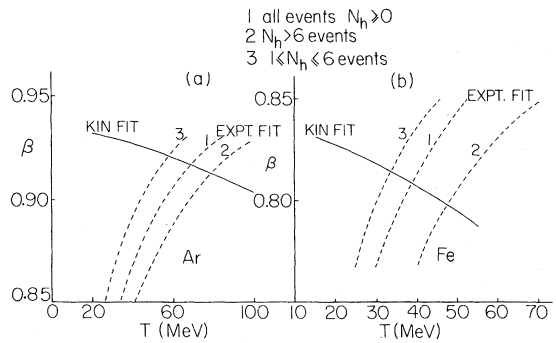

FIG. 6. β, T plots (a) Ar reactions at 2A GeV and (b) Fe reactions at 0.9A GeV. Kinematical fits are from relations 7 and 8. Experimental fits are fit to the tails of the experimental distributions (1), (2), and (3) which represent samples with $N_h\geq 0$, $N_h>6$, and $1\leq N_h\leq 6$, respectively.

cleon (0.931 GeV). $E_{\text{c.m.}}$ and ϵ (excitation energy) can be calculated from

$$E_{\text{c.m.}}=[E_L{}^2-p_L{}^2]^{1/2},$$

$$\epsilon=\frac{E_{\text{c.m.}}}{N_p+N_t}-m,$$

where m is taken to be 0.938 GeV, the mass of the free nucleon. t can be related to temperature by the nonrelativistic relation

$$\epsilon=\tfrac{3}{2}T. \tag{8}$$

The assumption of complete thermalization allows us to use the same value of temperature T for α particles. The values of β and T calculated for various combinations of N_p and N_t are shown in Fig. 6 as curves denoted by "KIN FIT."

The intersection of the two curves, EXPT FIT and KIN FIT, gives the kinematically allowed values of β_t and T_t of the fireball that fit the tail region of an angular distribution. The Boltzmann distribution corresponding to β_t and T_t is extrapolated for angles beween 0 and θ_p, and the extrapolated distribution is subtracted from the experimental numbers of the histogram. The resulting numbers in the peak area are fitted to the Boltzmann distribution, using the velocity β as β_p, the velocity of the projectile, and keeping T as free parameter. The value of T giving the best fit for the peak is termed T_p. Thus one gets β_t and T_t for the fireball which explains the tail area and β_p and T_p for the fireball which explains the peak area.

Such an analysis is done for every angular distribution shown in Figs. 3–5; the resulting values of β_t, T_t, β_p, and T_p are given in Table II. The values of these parameters obtained for similar angular distributions for ^{56}Fe-emulsion reactions at 1.7A GeV are also given for comparison.

D. Separation of events responsible for the tail part

From the analysis of a general sample of events as shown above, there exist two thermal sources; one (7–10 MeV) representing α particles from the projectile or projectile spectator breakup, while the other source (40–70 MeV) formed by a fireball mechanism with an N_p/N_t ratio corresponds to the tail part; thus they give two different distributions. It is important to ask at this point whether such a mixture of temperatures occurs in each event or the events fall in either one or the other of two distinct classes of temperatures. In order to answer this question, we looked at the angular distribution of α particles for all N_h in Figs. 4(a) and 4(b) for Ar and Fe. The tail part is slightly heavier in Fe reactions than in Ar reactions. Thus we chose Fe reactions at $\sim$0.9A GeV/nucleon for analysis in this section. As a first step towards isolation of events responsible for the tail part, we look at the dependence of angular distributions on the multiplicity of α particles, i.e., N_α. Figures 7(a)–7(c) illustrate events with $N_\alpha=1,2$, $N_\alpha=3,4$, and $N_\alpha>4$, respectively. We notice that the tail is heavier when N_α has intermediate values, i.e., $N_\alpha=3,4$ [Fig. 7(b)]. In angular distributions shown in Figs. 7(a) and 7(c) for $N_\alpha=1,2$ and $N_\alpha>4$, the tail was observed to be lighter. The N_h distributions for the respective events are shown in Figs. 7(d)–7(f). R_{tp} values for three samples and the percentage of events in each of the N_h groups are given in Table III. As can be seen, events with $N_\alpha=3,4$ which are richer in tail are also richer in large values of N_h, and have comparatively more target fragmentation. Thus the observations of events with only large N_h values approximately indicate the type of collision.

In Sec. III B, it was pointed out that R_{tp} is greater for larger values of N_h. This fact, when combined

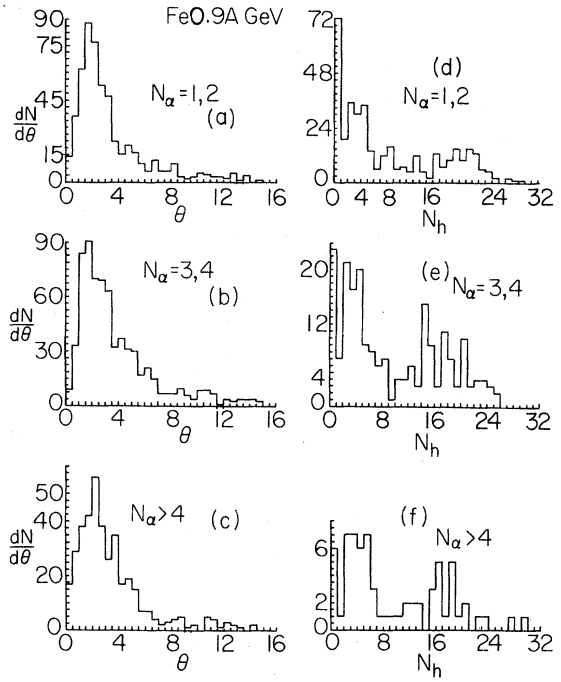

FIG. 7. Histograms in (a), (b), and (c) give space angle distributions for samples with $N_\alpha=1,2$, $N_\alpha=3,4$, and $N_\alpha>4$, respectively. (d), (e), and (f) give N_h distributions for the corresponding samples (Fe at 0.9A GeV).

TABLE III. Parameters for different groups based upon N_α.

Sample definition	R_{tp}	Percentage of events with $N_h=0$	$1 \le N_h \le 6$	$N_h > 6$
$N_\alpha=1,2$	0.313±0.028	19.1	36.7	44.1
$N_\alpha=3,4$	0.483±0.033	11.0	39.0	50.0
$N_\alpha>4$	0.342±0.035	8.8	45.6	45.6
$N_\alpha \ge 1$	0.387±0.019	15.4	38.4	46.2

with the fact that R_{tp} for $N_\alpha=3,4$ events is greater, leads to the conclusion that events with $N_h>6$ and $N_\alpha=3,4$ should have still heavier tails. Figure 8 shows such a separation, in that Fig. 8(a) shows the angular distribution for $N_\alpha=3,4$ and $N_h>6$, whereas the angular distribution for the rest of the events is shown in Fig. 8(b). The tails of both these distributions are fitted to Boltzmann distributions [Eq. (6)] in a manner described in Sec. III C; the parameters of the respective curves and R_{tp} values are also shown in the figure. Higher values of R_{tp} and T for Fig. 8(a) support the fact that this attempt is partially successful. This fact is further supported by the fact that the remnant peak area is much smaller for Fig. 8(a) than that for Fig. 8(b).

Another possibility will be to look at those events which have at least one α particle in the tail region with $\theta_{\max}>4°$, i.e., transverse momentum exceeding 100 MeV/c. Figure 9(a) shows the angular distribution of such events, whereas the N_h distribution for these events is shown in Fig. 9(b). In this figure, the N_h distribution is also compared to the N_h distribution for the whole sample (the dotted curve normalized to the same number of events). It is clear that events which have α tracks in the tail area are richer in larger N_h values, indicating that events responsible for the tail have larger target fragmentation also. The angular distribution of Fig. 9(a) is fitted

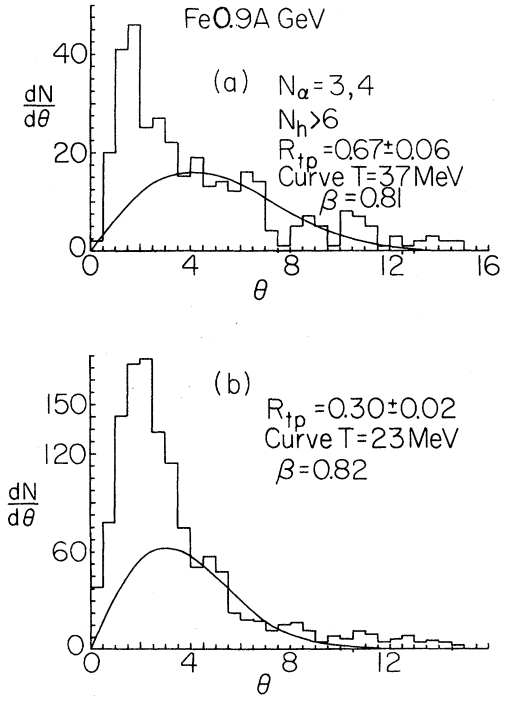

FIG. 8. Histograms show space angle distributions for (a) $N_\alpha=3,4$ and $N_h>6$, and (b) for rest of the events. The curves show calculations based upon relation (6). The curve in (a) corresponds to $T=37$ MeV and $\beta=0.81$, and in (b) is for $T=23$ MeV and $\beta=0.82$ (Fe at 0.9A GeV).

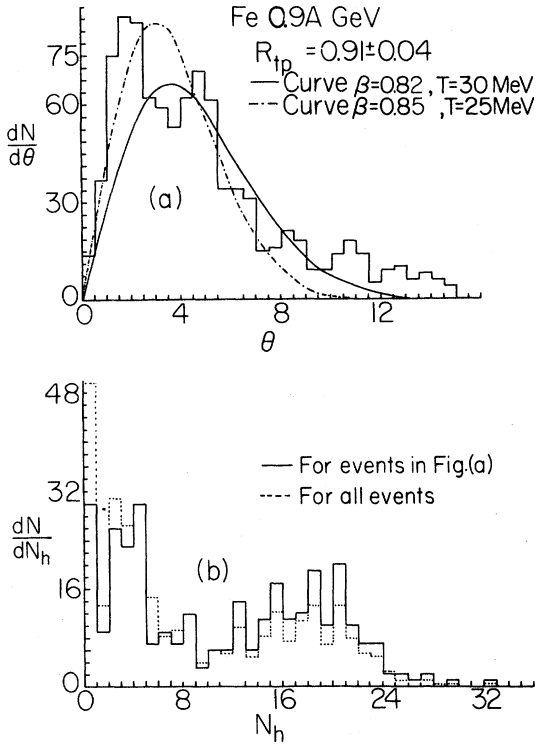

FIG. 9. (a) Space angle distributions for events which have at least one track with $\theta>4°$. (b) N_h distribution (full line) for the same events. Dotted line distribution shows the N_h distribution for all events, normalized to the same number. The curves in (a) are fits [relation (6)]; full line fit is the tail region ($T=30$ MeV and $\beta=0.82$) and extend to the peak area, and dotted line fit is the experimental distributions from 0° to 8° and then extended to higher angles ($T=25$ MeV and $\beta=\beta_p$) (Fe at 0.9A GeV).

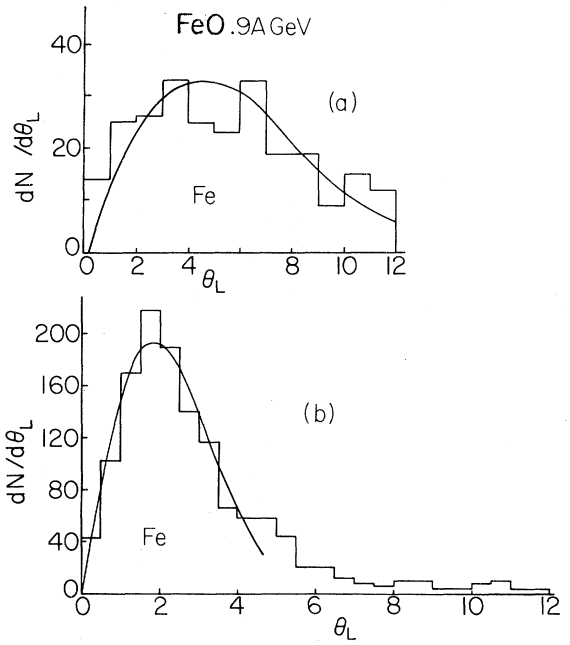

FIG. 10. (a) Angular distribution for all events for Fe at $0.9A$ GeV with $Z_F \leq 5$, $\Sigma Z_F < 10$, and $\theta \geq 5°$; the curve corresponds to $T = 45$ MeV and $\beta = 0.79$. (b) Angular distribution for events with $Z_F > 5$; the curve corresponds to $\beta = \beta_p$ and $T = 10$ MeV.

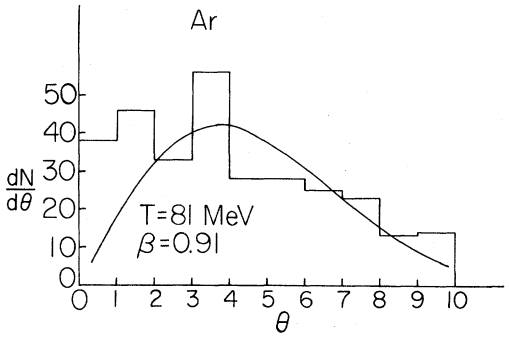

FIG. 11. Angular distribution for all events with $N_\alpha \leq 3$ and $\theta_{max} > 3°$ for Ar-emulsion interactions at $2A$ GeV; the curve corresponds to $T = 81$ MeV and $\beta = 0.91$.

to the predictions of the Boltzmann distribution. The full line curve is obtained by fitting the tail part and then extrapolating it to the peak area ($T = 30$, $\beta = 0.82$), whereas the dotted line curve is obtained by fitting to the experimental members from $0°-8°$ and then extrapolating it to higher angles ($T = 25$ MeV, $\beta = \beta_p$). Both these distributions give a fairly good description of the experimental distribution; in one a little portion of the peak seems to be left and in the other a little portion of the tail is left.

In Fig. 10 another attempt to separate tail type of events, where selection criteria include constraints on fragmentation products as well as the maximum angle of α particles is shown. Figure 10(a) shows events with $Z_F \leq 5$, where Z_F is the charge of a fragment, $\Sigma Z_F < 10$, and $\theta_{max} > 5°$, i.e., transverse momentum exceeding 130 MeV/c, whereas Fig. 10(b) is for all events with $Z_F > 5$. Here ΣZ_F is the sum of all the charges of the projectile fragments with $Z \geq 2$. Thus ΣZ_F represents the degree of projectile excitation. It can be seen that the distribution in Fig. 10(a) is a broad distribution without a peak, which can be fitted to one Boltzmann distribution, $T = 45$ MeV and $\beta = 0.79$. On the other hand, Fig. 10(b) shows that simply one criterion of the presence of heavy fragment Z_F decreases the tail part appreciably; this is clearly shown by the theoretical fit to the peak area ($\beta = \beta_p$, $T = 10$ MeV). In Fig. 11 we show an α-angular distribution for Ar at $\sim 2A$ GeV for events with $N_\alpha \leq 3$ and $\theta_{max} > 3°$. The Boltzmann distribution fit with the minimum χ^2 value gives $T = 81$ MeV and $\beta = 0.91$.

IV. CONCLUSIONS

Projectile fragmentation studies of Ar and Fe show that relativistic α particles get slightly larger transverse momenta than observed in C, N, and O reactions. Deduced values of $\sigma(p)$, p_f, and T also show a similar trend.

The variation of the angular distribution is explained by the following:

(a) For heavy projectiles Fe and Ar the angular distribution of α particles, and so in general the fragmentation of the projectile, is not influenced by the target or target fragmentation.

(b) As expected, the tail is slightly lighter for Ar reactions than for the Fe reaction. Angular distributions of relativistic α particles in Fe reactions at $0.9A$ GeV behave in a similar manner as observed earlier in Fe reactions at $1.7A$ GeV.

(c) Comparison of the angular distributions with the predictions from a moving relativistic Boltzmann distribution shows that the general angular distributions can be imagined to consist of two distributions. One distribution represents the peak area as usual for a thermal source moving with projectile velocity β_p and excited to low temperatures (7—10 MeV). The other that fits the tail

area is for thermal sources heated to much higher temperatures (30–80 MeV); these sources are also moving with velocities slightly smaller than β_p.

An attempt to analyze and separate tail-type events has led to the following conclusions:

(a) R_{tp} is greater for intermediate values of N_α, i.e., 3,4; these events are also richer in higher N_h values.

(b) A combined constraint on N_α and N_h values ($N_\alpha = 3,4$ and $N_h > 6$) enriches the tail portion and decreases the tracks in the peak area.

(c) Isolation of the events which have large angle alphas ($\theta_{\max} > 4°$), and their fit to the Boltzmann show that attempts to explain experimental angular distribution by one distribution leaves only a small portion of peak or tail, depending upon the fitting constraints. These events have a larger fraction of events with higher N_h values than the general sample.

(d) The angular distribution depends upon the charge of the remaining projectile fragment. A combined constraint on fragmentation products ($Z_F \leq 5$, $\Sigma Z_F < 10$) and angle of one of the α particles greater than 5° separates a sample of events which can be described by a single Boltzmann distribution [Fig. 10(a)].

(e) The separation is again possible in Ar-em interaction if we take events with $N_\alpha \leq 3$ and the angle of one of the α particles greater than 3° which is shown in Fig. 11. Thus a large transverse momentum transfer may explain the tail at high temperature.

ACKNOWLEDGMENTS

We are very grateful to the staff of Bevalac at Lawrence Berkeley Laboratory for their help with the exposure of emulsion stacks and to Vandana Rani for her help in scanning. This work was supported in part by Grant No. R01CA2487802 that was awarded by the National Cancer Institute, U. S. Department of Health, Education, and Welfare, and the State University of New York at Buffalo, Research Development Funds and Incentive Funds from the Research Foundation of SUNY.

[1]P. L. Jain and G. Das, Phys. Rev. Lett. 48, 305 (1982).
[2]P. L. Jain, M. M. Aggarwal, G. Das, and K. B. Bhalla, Phys. Rev. C 25, 3216 (1982).
[3]D. E. Griener *et al.*, Phys. Rev. Lett. 35, 152 (1975); H. H. Heckman, D. E. Griener, P. J. Lindstrom, and H. Shwe, Phys. Rev. C 17, 1735 (1978).
[4]J. V. Lepore and R. J. Riddell, Jr., Lawrence Berkeley Laboratory Report No. LBL-3086, 1974 (unpublished).
[5]H. Feshback and K. Huang, Phys. Lett. 47B, 300 (1973).
[6]A. S. Goldhaber, Phys. Lett. 53B, 306 (1974).
[7]E. J. Moniz *et al.*, Phys. Rev. Lett. 26, 445 (1971).
[8]K. B. Bhalla *et al.*, Nucl. Phys. A367, 446 (1981).
[9]J. Gosset *et al.*, Phys. Rev. C 16, 1629 (1977); L. D. Laudau and E. M. Lifshitz, *Statistical Physics* (Addison-Wesley, New York, 1969), p. 109; S. I. A. Garpman, Phys. Lett. 106B, 367 (1981).